J Solid State Electrochem (2009) 13:301–307
DOI 10.1007/s10008-008-0533-3

Synthesis and electrochemical characterizations of nano-crystalline $LiFePO_4$ and Mg-doped $LiFePO_4$ cathode materials for rechargeable lithium-ion batteries

D. Arumugam · G. Paruthimal Kalaignan · P. Manisankar

Received: 18 December 2007 / Revised: 7 February 2008 / Accepted: 14 February 2008 / Published online: 8 March 2008

Abstract Nano-crystalline $LiFePO_4$ and $LiMg_{0.05}Fe_{0.95}PO_4$ cathode materials were synthesized by sol–gel method in argon atmosphere using succinic acid as a chelating agent. Physico-chemical characterizations were done by thermo-gravimetric and differential thermal analysis, X-ray diffraction, scanning electron microscopy, transmittance electron microscopy, and Raman spectroscopy. Electrochemical behavior of the cathode materials were analyzed using cyclic voltammetry, and galvanostatic charge/discharge cycling studies were employed to characterize the reaction of lithium-ion insertion into and extraction from virginal and magnesium-doped $LiFePO_4$, in the voltage range 2.5 to 4.5 V (Vs Li/Li^+) using 1 M $LiPF_6$ with 1:1 ratio of ethylene carbonate and dimethyl carbonate as electrolytes. $LiMg_{0.05}Fe_{0.95}PO_4$ exhibits initial charge and discharge capacities of 159 and 141 mAh/g at 0.2 C rate respectively, as compared to 121 and 107 mAh/g of pristine $LiFePO_4$. Furthermore, $LiMg_{0.05}Fe_{0.95}PO_4$ has retained more than 89% of the capacity even after 60 cycles. Hence, $LiMg_{0.05}Fe_{0.95}PO_4$ is a promising cathode material for rechargeable lithium-ion batteries.

Keywords Lithium-ion batteries · $LiFePO_4$ · $LiMg_{0.05}Fe_{0.95}PO_4$ · Sol–gel method · TG/DTA · XRD · SEM · TEM · Raman spectroscopy · Cyclic voltammetry · Galvanostatic charge/discharge

D. Arumugam · G. Paruthimal Kalaignan (✉) · P. Manisankar
Advanced Lithium-Ion Battery Research Lab,
Department of Industrial Chemistry, Alagappa University,
Karaikudi 630 003, India
e-mail: pkalaignan@yahoo.com

Introduction

Intensive work has been dedicated to transition metal oxides like $LiCoO_2$, $LiNiO_2$, and $LiMn_2O_4$ as the positive electrode materials in secondary lithium-ion batteries. Substitution of cobalt, nickel, and manganese by other metals has been studied in order to improve the electrochemical performance, mainly focused on obtaining larger capacity and high voltage. In this way, several studies have been recently reported concerning the phosphate system $LiMPO_4$ (M=Fe, Ni, Co, etc) with olivine-related structure. The olivine structure of $LiFePO_4$ could be used as cathode material for lithium-ion batteries since 1997 [1, 2]. It has been widely investigated as a promising cathode material to replace the high-cost $LiCoO_2$. In addition, it is more abundant and environmentally benign [3]. Besides, it has theoretical capacity of 170 mAh/g [2], discharge potential of 3.5 V Vs Li/Li^+ [4], and excellent thermal stability [5, 6]. $LiFePO_4$ can be synthesized by normal solid-state reaction. Unfortunately, it is very difficult to achieve the theoretical capacity of $LiFePO_4$ because of its low electrical conductivity and slow diffusion of lithium ions in the olivine structure [1, 4, 7]. So far, several alternative methods have been applied for the preparation of lithium iron phosphate cathode material. There are a lot of methods to synthesize the pure $LiFePO_4$, for instance hydrothermal method [8–10], microwave method [11], sol–gel method [3, 12–14], spray pyrolysis [15], emulsion drying method [16], co-precipitation technique [17], soft chemistry route [18], and other unusual approaches such as pulsed-layer deposition [19] and template technology [20]. In the early period of research, its reversible capacity has reached only 60% of the theoretical capacity, namely, the deintercalation of only 0.6 lithium atoms in $LiFePO_4$. The limited intercalation and deintercalation process was mainly due to its poor con-

ductivity [1, 3]. Among various attempts to enhance the electrical conductivity, carbon coating is a common way to overcome the limited rate capacity because the dispersed carbon particles provide pathways of electron transfer resulting in improvement of the conductivity and electrochemical properties [21–25]. $LiFePO_4$ has an ordered olivine-type structure (space group Pmnb) in which Li, Fe, and P atoms occupy octahedral 4a, 4c, and tetrahedral 4c sites [26]. The alien atom (Zn, Ti, and Zr) doping has been adopted to modify the electrochemical performances of olivine-type $LiFePO_4$ cathode materials of lithium-ion batteries [27]. The electrochemical conductivity of $LiFePO_4$ can be improved by dispersing copper/silver powders [13] or high surface area carbon black [28] and doping with alien ion [7].

In this paper, we have reported for the first time magnesium-doped nano-crystalline lithium iron phosphate material to form homogeneous $LiMg_{0.05}Fe_{0.95}PO_4$ by sol–gel method using succinic acid as a chelating agent, and the doping effect was investigated.

Experimental

Virginal and magnesium-doped nano-crystalline lithium iron phosphate samples were prepared by a low-temperature sol–gel technique. All the starting material like $LiNO_3$, $Fe(OCOCH_3)_2.4H_2O$, $Mg(NO_3)_2.4H_2O$, and $NH_4H_2PO_4$ were dissolved in triple-distilled water. The resultant solution was mixed with appropriate amount of succinic acid. Weak acid or neutral or weak basic precursor solutions are preferable to obtain single phase of $LiFePO_4$ [11]; strong basic condition should be avoided to prepare $LiFePO_4$ without impurity phase [29]. So the pH of the solution was adjusted, ranging between 5.0 and 5.5 using liquid NH_3. The resulting homogeneous cleared solution was heated (60 °C) with continuous stirring. The highly viscous gel was obtained after 7 h, and then it was dried overnight at 110 °C in inert atmosphere to decompose the nitrate and acetate groups. Finally, the precursor was sintered at different temperatures (250, 400, 600, and 850 °C) for 15 h in an argon atmosphere to prevent the oxidation of Fe^{2+} to Fe^{3+} [30].

Thermal decomposition behavior of the gel precursor was examined by thermogravimetric analysis and differential thermal analysis in argon flow between the temperatures 0 and 700 °C at a heating rate of 10 °C/min (Simultaneous thermal analysis polymer laboratory, thermal science division; UK model: STA 15000). Structure and crystallinity of the synthesized powders were measured using a Shimadzu XRD-6000 X-ray diffractometer with Cu-Kα radiation. Data were collected in the range of 10–60° at a scan rate of 1°/min. The surface morphology and microstructure of powder particles were characterized by scanning electron microscopy (SEM HITACHI S-3000H) and transmittance electron microscopy (TEM). Room temperature laser Raman spectrum was recorded for the synthesized pristine $LiFePO_4$ as well as magnesium-doped lithium iron phosphate using Jobin-Yvon ISA T64000 Raman spectrometer equipped with a charge-coupled device detector and a microscope. Powder samples were put under microscope objective that allows the laser beam to focus on a small selected area of the surface (~1 μm^2), and the backscattered Raman signal was collected. The laser light source was 514.5 nm, line excited at 5–10 mW at an argon laser power. All the Raman spectra were recorded over the frequency range 100–1200 cm^{-1} at an acquisition time of 400 s and were arranged to increase the signal-to-noise ratio. The cathodes were prepared by mixing with 85 wt% of active material (synthesized at 850 °C), 10 wt% of acetylene black as a conducting material, and 5 wt% of polyvinylidene difluoride as a binder in *N*-methyl-2-pyrrolidinone solvent to form homogeneous slurry. Then the slurry was coated onto an aluminum foil and cut into 22 mm

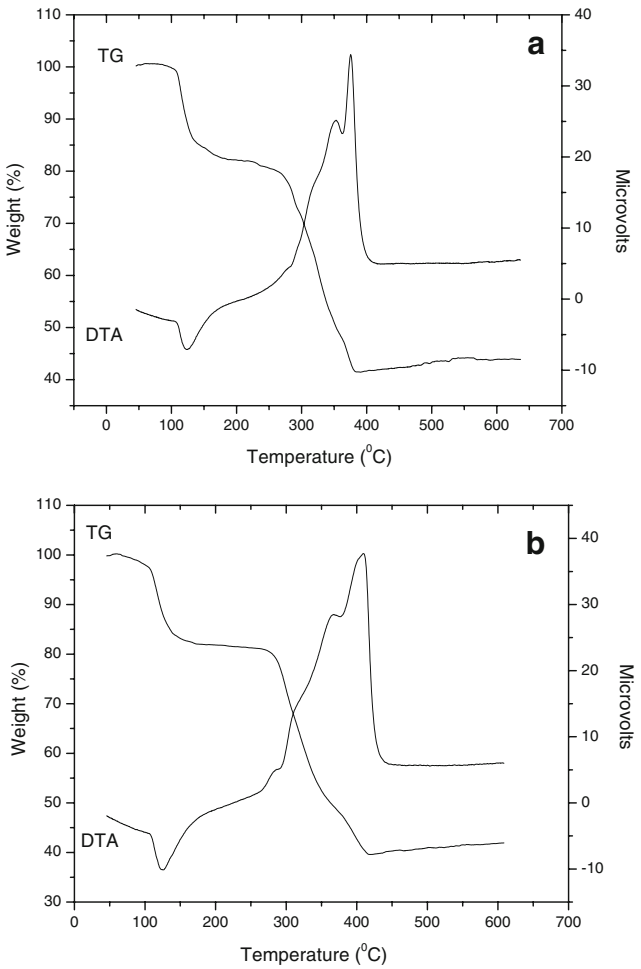

Fig. 1 TG/DTA curves of **a** virginal lithium iron phosphate and **b** Mg-doped lithium iron phosphate

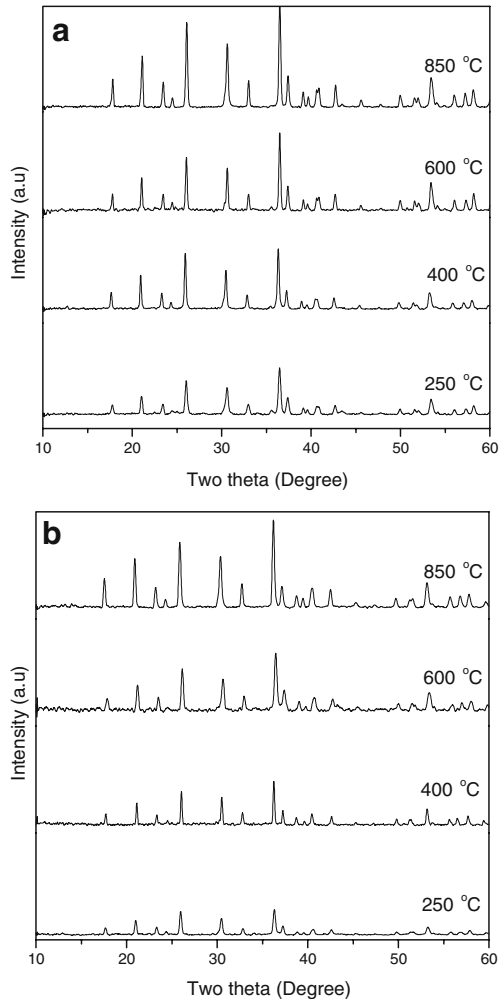

Fig. 2 X-ray diffraction patterns of **a** Virginal $LiFePO_4$ **b** Mg-doped $LiFePO_4$ synthesized at different temperatures

diameter and then dried by vacuum oven at 120 °C for 12 h. Finally, coin-type cells were assembled in a glove box (Braun unilab, Germany 2002), which used lithium foil as the counter electrode, celgard 2400 as the separator, and $LiPF_6$ mixed with 1:1 ratio of ethylene carbonate and dimethyl carbonate as the electrolyte. The electrochemical properties of the cells were characterized using cyclic voltammetry at a scan rate of 0.01 mV/s and galvanostatic charge and discharge studies over a voltage range of 2.5–4.5 V at 0.2 C rate.

Results and discussion

Thermogravimetric and differential thermal analysis

Thermal decomposition of the gel precursors were examined by means of the thermogravimetric and differential thermal analysis. Figure 1a and b represent the thermogravimetric and differential thermal analysis (TG/DTA) curves of $LiFePO_4$ and magnesium-substituted $LiFePO_4$ precursors. They exhibited one endothermic peak centered at around 100–150 °C and one exothermic peak centered at 250–450 °C. The endothermic event corresponding to a weight loss of 20% may be ascribed to the removal of water. The exothermic peak was combined with huge weight loss of 40% that appeared from 250 to 450 °C, which was assigned to the formation of the compound. Gravimetric stable behaviors observed beyond 450 °C confirm the completion of thermal event.

X-ray diffraction analysis

The X-ray diffraction pattern of virginal and magnesium-doped $LiFePO_4$ are shown in Fig. 2a and b. All diffraction lines are indexed to an orthorhombic olivine structure (space group Pmnb). The peak intensity of the X-ray diffraction pattern of both doped and undoped $LiFePO_4$ was enhanced with increase in the calcinations temperature, which ascribed to improve the degree of crystallinity, and no impurity phase was detected at high temperature (850 °C) from X-ray diffraction. We intended to substitute the dopant ions Mg^{2+} for Fe^{2+} on the M_2 sites in the olivine structure. A previous report found the detectable impurity of Li_3PO_4 in doped $LiZn_xFe_{1-x}PO_4$ prepared by solid state reaction even at very low dopant level [7]. In contrast, detectable precipitation of Li_3PO_4 impurity was not formed in the synthesized $LiMg_{0.05}Fe_{0.95}PO_4$ compound using sol–gel method. During the synthesis process, the reactants were mixed homogeneously in the solution and then formed gel complex. Therefore, the homogeneous distribution of composition elements are expected [3]. The X-ray diffraction (XRD) curves of the doped materials exhibit a minute leftward shift in the axis of 2θ compared with the virginal one, indicating an influence of lattice parameter [31, 32]. The lattice parameters were calculated and summarized in Table 1. Mg-doped LiFePO4 has higher lattice constants of

Table 1 Calculated lattice parameters and unit cell volume of the $LiFePO_4$ and $LiMg_{0.05}Fe_{0.95}PO_4$

Samples	Space group	Lattice constant 'a' (Å)	Lattice constant 'b' (Å)	Lattice constant 'c' (Å)	Unit cell volume (Å^3)
$LiFePO_4$	Pmnb	5.9601	10.2035	4.7183	286.94
$LiMg_{0.05}Fe_{0.95}PO_4$	Pmnb	6.0351	10.2865	4.7293	293.60

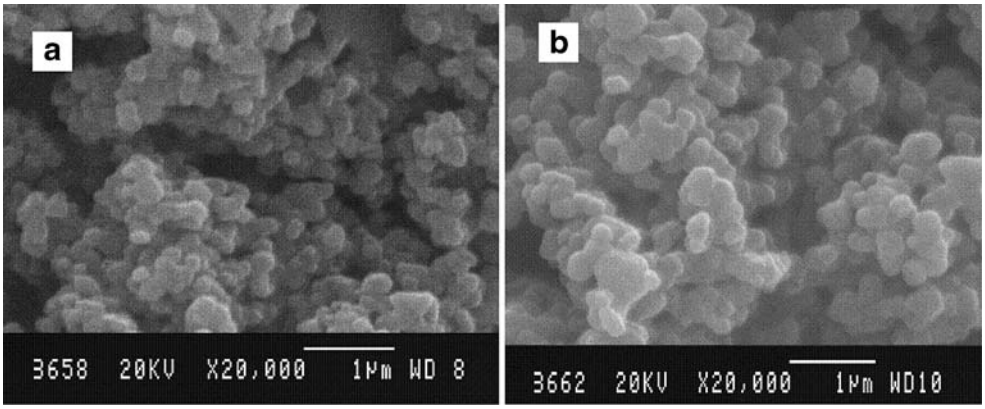

Fig. 3 Scanning electron micrographs of **a** $LiFePO_4$ and **b** $LiMg_{0.05}Fe_{0.95}PO_4$ cathode materials synthesized at 850 °C

a, b, and c than virginal one and enlarges the total volume of the unit cell for about 2.27%.

Scanning and transmittance electron microscopy

The surface morphology and particle size of the virginal and magnesium-doped lithium iron phosphate samples are shown in Figs. 3 and 4. SEM micrographs in Fig. 3 show that the product particles are spherical, their diameter is about 0.1–0.5 μm, and TEM image in Fig. 4 shows both virginal and doped $LiFePO_4$ have particles size around 50–100 nm, and the particles are loosely agglomerated. The small particles and loosely agglomerated structure allow easy penetration of the electrolyte and provide a short pathway for lithium-ion diffusion in the active materials.

Raman spectroscopy

The olivine structure belongs to the spectroscopic group D_{2h}^{16}; the primitive cell is centrosymmetric with formula units in the cell. Li, Fe, and P atoms are distributed on 4a, 4c, and 4c position (wyckoff notation), respectively. As the structure of the phospho olivine builds from LiO_6 and MO_6 octahedral linked to PO_4^{3-} tetrahedral polyanions, the local cationic arrangement can be discussed with factor group analysis and the molecular vibration modes [33]. In this work, Fig. 5a represents Raman spectrum of phospho olivine $LiFePO_4$; five bands were observed around 947, 1,009−1,070, and 580−640 cm^{-1}. The very sharp band with higher intensity located at 947 cm^{-1} is ascribed to A_g symmetric P−O stretching vibration mode, and two weaker bands between 1,009 and 1,070 cm^{-1} belong to antisymmetric stretching vibration modes of the PO_4^{3-} anion in phospho olivine $LiFePO_4$ [34]. The bands around 589−640 and 464 cm^{-1} were attributed to A_{1g} symmetric of Fe−O stretching and bending vibration of Fe−O−P groups in $LiFePO_4$ [35]. Figure 5b is the magnesium-doped $LiFePO_4$. Both virginal and magnesium-doped $LiFePO_4$ have no change in vibration modes and intensity of the Raman spectra, which depicts no structural change of $LiFePO_4$ with 0.05 magnesium content.

Cyclic voltammetry

Typical cyclic voltammograms of the virginal $LiFePO_4$ and magnesium-doped $LiFePO_4$ cathode materials are given in Fig. 6; lithium foil acts as counter and reference electrodes. The cyclic voltametric curves indicated that the potential

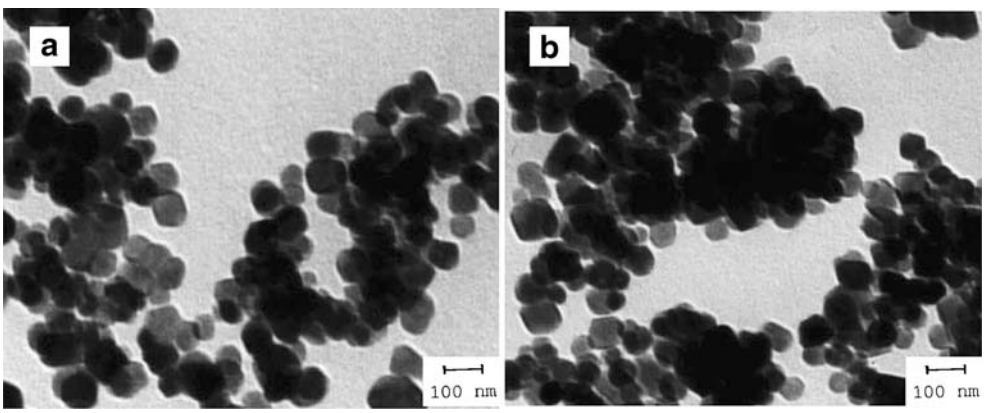

Fig. 4 Transmittance electron micrographs of **a** $LiFePO_4$ and **b** $LiMg_{0.05}Fe_{0.95}PO_4$ cathode materials synthesized at 850 °C

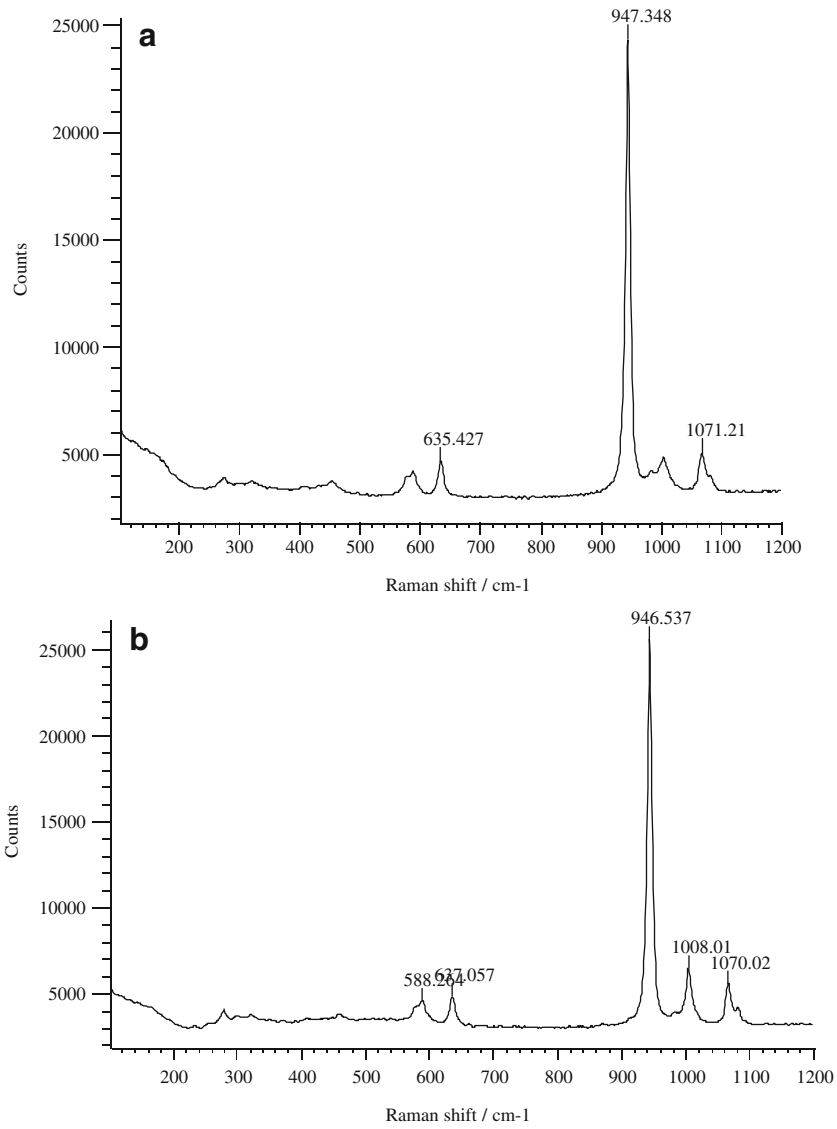

Fig. 5 Raman spectra of **a** $LiFePO_4$ and **b** $LiMg_{0.05}Fe_{0.95}PO_4$ cathode materials, which were synthesized at 850 °C

range in which the lithium deintercalation/intercalation occurs and the phase transition (if there is any) also formed during this process. All measurements were taken at room temperature at a scan rate 0.01 mV/s and the voltage range from 2.5 to 4.5 V Vs Li/Li^+. The $LiFePO_4$ and $LiMg_{0.05}Fe_{0.95}PO_4$ cathodes gave a single anodic peak during the charge at 3.52 and 3.54 V, respectively. This corresponds to single-step lithium-ion removal from the cathode materials. The single cathodic peak was obtained at 3.15 and 3.38 V for $LiFePO_4$ and $LiMg_{0.05}Fe_{0.95}PO_4$, respectively, which corresponds to Li^+ reinsertion into cathodes. The cyclic voltammetry curve of magnesium-doped $LiFePO_4$ shows more symmetrical and sharper shape of the anodic and cathodic peaks. The bigger voltammetric peaks are observed for the Mg-doped materials compared to that of undoped both in the anodic and cathodic runs, which also indicated the enhancement of the lithium-ion diffusion. In the case of $LiMg_{0.05}Fe_{0.95}PO_4$, the peak potential difference

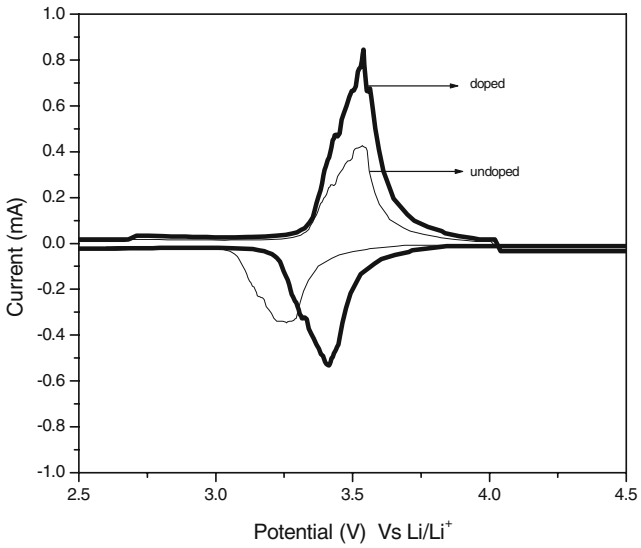

Fig. 6 Typical cyclic voltammetry curves of doped and undoped $LiFePO_4$ at scan rate of 0.01 mV/s

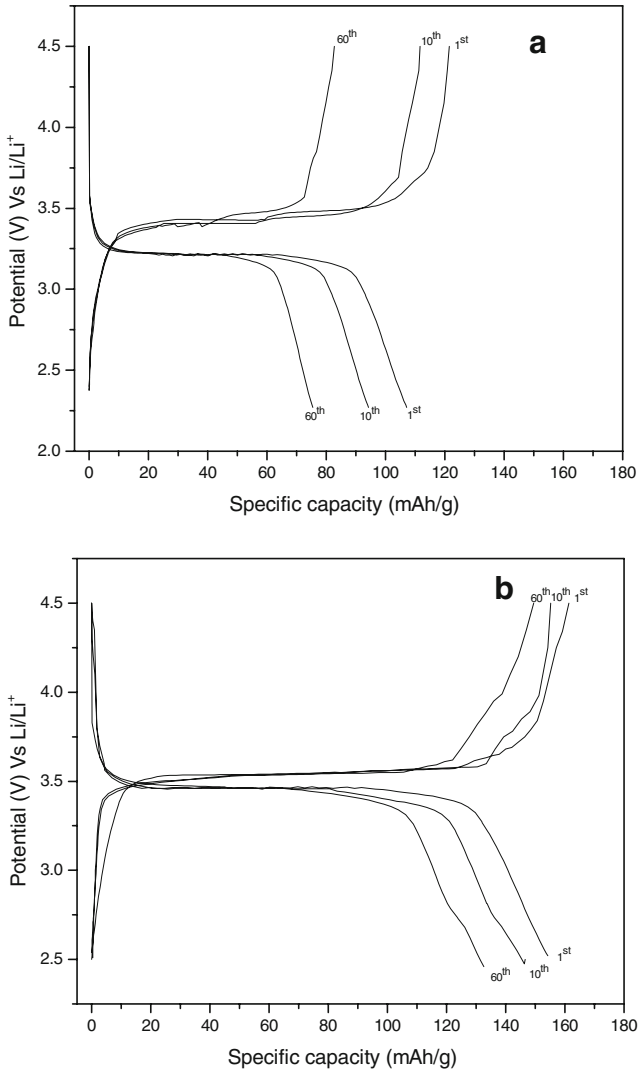

Fig. 7 Galvanostatic charge and discharge studies of 1st, 10th and 60th cycles over a voltage range of 2.5–4.5 V at 0.2 C rate for **a** $LiFePO_4$ **b** $LiMg_{0.05}Fe_{0.95}PO_4$

(ΔE_p) between anodic and cathodic peaks is 0.16 V, whereas that of undoped $LiFePO_4$ is 0.37 V. It revealed $LiMg_{0.05}Fe_{0.95}PO_4$ cathode has reversible/quasireversible nature of Li^+ transport in the electrochemical cell between $LiFePO_4$ and $FePO_4$ structure.

Charge/discharge performance

Figure 7a and b represent the charge/discharge voltage profiles of $LiFePO_4$ and Mg doped $LiFePO_4$ electrodes. The cells were galvanostatically charged and discharged at C/5 rate with a current density of 0.19 mAh/g between voltages of 2.5 and 4.5 V. Initial charge and discharge capacity of virginal $LiFePO_4$ has 121 and 107 mAh/g, respectively. For magnesium-doped lithium iron phosphate, the charge capacity increases from 121 to 159 mAh/g, and the discharge capacity from 107 to 141 mAh/g approaching the theoretical capacity of 170 mAh/g. The virginal $LiFePO_4$ exhibits flat charge and discharge plateau around 3.52 and 3.15 V, respectively. The potential around 3.54 and 3.38 V are corresponding to charge and discharge plateaus of Mg-doped $LiFePO_4$, which is identified as the single-phase transition process between $LiFePO_4$ and $FePO_4$ phase. $LiMg_{0.10}Fe_{0.90}PO_4$ has larger charge and discharge capacity compared to virginal $LiFePO_4$, which ascribed to magnesium-doped lithium iron phosphate and has improved the electrical conductivity and larger lithium-ion diffusion from the active materials.

Cycling performance

The cycling performances of the $LiFePO_4$ and magnesium-doped $LiFePO_4$ samples were evaluated in the voltage range of 2.5 to 4.5 V at room temperature in the cell configuration $Li/LiFePO_4$, and the results are shown in Fig. 8. As shown in Figs. 7 and 8, the initial discharge capacity of pristine $LiFePO_4$ material is about 107 mAh/g; after 60 cycles, the discharge capacity is 75 mAh/g. The initial discharge capacity of magnesium-doped $LiFePO_4$ is 141 mAh/g; after 60 cycles, the discharge capacity was decreased from 141 to 132 mAh/g. Initial discharge capacity of magnesium-doped lithium iron phosphate is higher than pristine $LiFePO_4$ due to larger lithium-ion diffusion from active materials. The magnesium-doped $LiFePO_4$ material has excellent cycling behavior with little discharge capacity loss after 60 cycles. The capacity loss is less than 9%. In comparison, the capacity loss of the $LiFePO_4$ electrode is 30% after 60 cycles. The magnesium-doped $LiFePO_4$ has improved the reversible capacities as

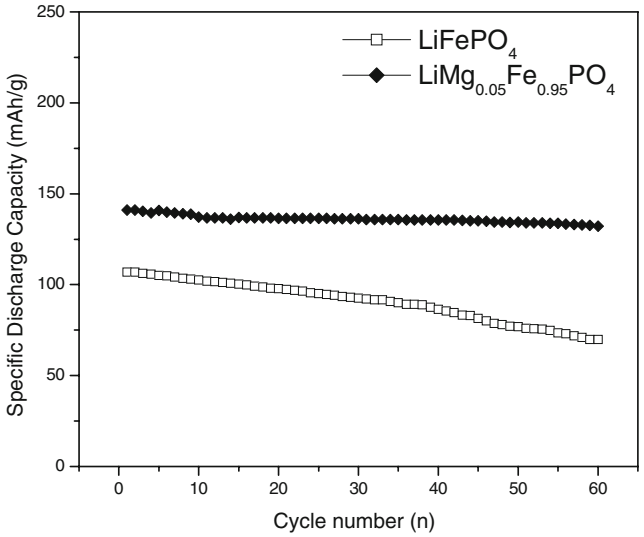

Fig. 8 Comparison between the charge/discharge cycling behaviors of virginal and Mg-doped $LiFePO_4$ samples at 0.2 C rate

well as the cycling performance due to larger crystal unit, and increasing the conductivity from doping, the movement of lithium ions, and the electronic transferring process in the Mg-doped $LiFePO_4$ are faster and more stable during the cycling process.

Conclusions

Mg-doped $LiFePO_4$ and virginal $LiFePO_4$ were synthesized by low-temperature sol–gel method using succinic acid as a chelating agent. The synthesized powder particles are spherical, and the size is around 50–100 nm. TG/DTA and XRD studies of the materials have confirmed that olivine-structured single-phase pure crystalline formed during the sol–gel treatment process. Raman spectra revealed that pure olivine structure of $LiFePO_4$ is attained at 0.05 magnesium doping without impurities. The magnesium doping favors the formation of the crystal structure, expands the lattice volume, and provides more space for lithium-ion intercalation and deintercalation. In addition, magnesium-doped $LiFePO_4$ has higher charge/discharge capacities, and the reversibility of lithium insertion into and removal from the cathode materials may be due to the enhancement of the electrical conductivity. As a result, Mg doping is very promising for the development of structural stability and improvement of electrochemical performance of $LiFePO_4$.

References

1. Padhi AK, Nanjundaswamy KS, Goodenough JB (1997) J Electrochem Soc 144:1188
2. Padhi AK, Nanjundaswamy KS, Masquelier C, Okada S, Goodenough JB (1997) J Electrochem Soc 144:1609
3. Wang GX, Bewlay S, Yao J, Ahn JH, Dou SX, Liu HK (2004) Electrochem Solid State Lett 7:A506
4. Yamada A, Chung SC, Hinokuma K (2001) J Electrochem Soc 148:A224
5. Delacourt C, Poizot P, Morerette M, Tarascon J, Masquelier C (2004) Chem Mater 16:93
6. Takahashi M, Tobishima S, Takei K, Sakuai Y (2002) Solid State Ionics 148:283
7. Chung SY, Bloking JT, Chiang YM (2002) Nat Mater 1:123
8. Yang SF, Zavalij PY, Whittingham MS (2001) Electrochem Commun 3:505
9. Yang SF, Song YN, Zavalij PY, Whitingham MS (2002) Electrochem Commun 4:239
10. Shiraishi K, Dokko K, Kanamura K (2005) J Power Sources 146:555
11. Higuchi M, Katayama K, Azuma Y, Yukawa M, Suhara M (2003) J Power Sources 119:258
12. Croce F, Epitanio AD, Hassoun J, Deptula A, Olczac T, Scrosati B (2002) Electrochem Solid State Lett 5:A47
13. Yang JS, Xu JJ (2004) Electrochem Solid State Lett 7:A515
14. Fu LJ, Liu H, Wu YP, Rahm E, Holze R, Wu HQ (2005) Prog Mater Sci 50:881
15. Bewlay SL, Konstantinov K, Wang GX, Dou SX, Liu HK (2004) Nat Mater Lett 58:1788
16. Cho TH, Chung HT (2004) J Power Sources 133:272
17. Park HS, Son JT, Chung HT, Kim SJ, Lee CH, Him HG (2003) Electrochem Commun 5:839
18. Prosini PP, Carewska M, Scaccia S, Wisniewski P, Pasquali M (2003) Electrochim Acta 48:4205
19. Song SW, Reade RP, Kostecki R, Striebel KA (2005) J Electrochem Soc 153:A12
20. Sides CR, Croce F, Young VY, Martin CR, Scrosati B (2005) Electrochem Solid State Lett 8:A484
21. Huang H, Yin SC, Nazar LF (2001) Electrochem Solid State Lett 4:A170
22. Ravet N, Choccinard Y, Magman JF, Besner S, Gauthier M, Armand M (2001) J Power Sources 97:503
23. Zaghib K, Shim J, Guerfi A, Charest P, Striebed KA (2005) Electrochem Solid State Lett 8:A207
24. Myang ST, Komaba S, Hirosak N, Yashiro H, Kumakai N (2004) Electrochim Acta 49:4213
25. Spong AD, Vitins G, Owen JR (2005) J Electrochem Soc 152: A2376
26. Streitsove VA, Belokoneva EL, Tsirelson VG, Hansen N (1993) Acta Crystallogr B Struct Sci 49:147
27. Liu H, Cao Q, Fu LJ, Li C, Wu YP, Wu HQ (2006) Electrochem Commun 8:1553
28. Prosini PP, Zane D, Pasquali M (2001) Electrochem Acta 46:3517
29. Lee J, Teja AS (2005) J Supercrit Fluids 35:83
30. JCPDS card No 40-1499
31. Liu H, Cao Q, Fu LJ, Li C, Wu YP, Wu HQ (2006) Electrochem Commun 8:1553
32. Nakamura T, Sakumoto K, Okamoto M, Seki S, Kobayashi Y, Takeuchi T, Tabuchi M, Yamada Y (2007) J Power Sources 174:435
33. Nakamura T, Mima Y, Tabuchi M, Yamada Y (2006) J Electrochem Soc 153:A1108
34. Burba CM, Frech R (2004) J Electrochem Soc 151:A1032
35. Paques-Ledent MT, Tarte P (1974) Spectrochim Acta Part A 30:673